ACS APPLIED MATERIALS & INTERFACES

Research Article

www.acsami.org

Flexible, Hybrid Piezoelectric Film ($BaTi_{(1-x)}Zr_xO_3$)/PVDF Nanogenerator as a Self-Powered Fluid Velocity Sensor

Nagamalleswara Rao Alluri,[†] Balasubramaniam Saravanakumar,[‡] and Sang-Jae Kim*[,‡,§]

[†]Department of Mechanical Engineering and [‡]Department of Mechatronics Engineering, Nanomaterials and System Lab, Jeju National University, Jeju 690756, Korea

[§]School of Materials Science and Engineering, Georgia Institute of Technology, Atlanta, Georgia 30332-0245, United States

Supporting Information

ABSTRACT: We demonstrate a flexible piezoelectric nanogenerator (PNG) constructed using a hybrid (or composite) film composed of highly crystalline $BaTi_{(1-x)}Zr_xO_3$ (x = 0, 0.05, 0.1, 0.15, and 0.2) nanocubes (abbreviated as BTZO) synthesized using a molten-salt process embedded into a poly(vinylidene fluoride) (PVDF) matrix solution via ultrasonication. The potential of a BTZO/PVDF hybrid film is realized in fabricating eco-friendly devices, active sensors, and flexible nanogenerators to interpret its functionality. Our strategy is based on the incorporation of various Zr^{4+} doping ratios into the Ti^{4+} site of $BaTiO_3$ nanocubes to enhance the performance of the PNG. The flexible nanogenerator (BTZO/PVDF) exhibits a high electrical output up to ~11.9 V and ~1.35 μA compared to the nanogenerator (BTO/PVDF) output of 7.99 V and 1.01 μA upon the application of cyclic pushing-releasing frequencies with a constant load (11 N). We also demonstrate another exciting application of the PNG as a self-powered sensor to measure different water velocities at an outlet pipe. The average maximum peak power of the PNG varies from 0.2 to 15.8 nW for water velocities ranging from 31.43 to 125.7 m/s during the water ON condition. This study shows the compositional dependence approach, fabrication of nanostructures for energy harvesting, and self-powered devices in the field of monitoring for remote area applications.

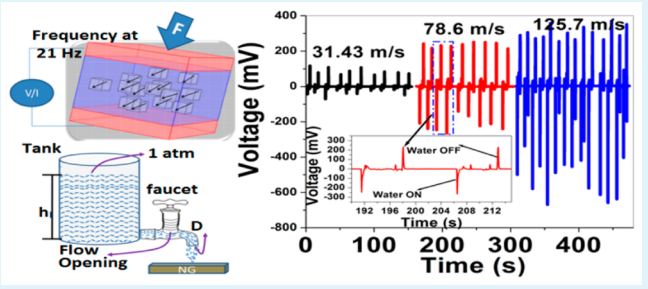

KEYWORDS: *piezoelectric nanogenerator, flexible, hybrid film, $BaTi_{(1-x)}Zr_xO_3$ nanocubes, self-powered sensor, molten salt process*

INTRODUCTION

Self-powered portable devices and active transducers play key roles at present, and will continue to do so in the near future, because they can function without any external bias voltage sources or additional processes.[1,2] Self-powered sensors of pH,[3] temperature,[4] vibration,[5] ethanol,[6] micro flow,[7] and water motion active transducers[8] have been intensely investigated and successfully implemented. Conventional battery-based sensors have several disadvantages, such as power consumption, large package size, high system cost,[9] and risk of environmental pollution,[1] resulting in the demand for new, alternative approaches including self-powered technology. The importance of this technology is based on driving a device or sensor by harvesting energy from piezoelectric,[10] triboelectric,[11] thermal gradient,[12] or solar methods.[13] The piezoelectric harvesting method[10,14] is the most promising of these methods because it is less affected by external conditions such as humidity and temperature. Nanogenerators using functional materials (piezoelectric ceramics with 3D, 2D, and 1D structures) have been developed as a disruptive innovation, generating voltage in response to mechanical force (and vice versa). Piezoelectric nanogenerators (PNGs) using ZnO,[10,15] PVDF,[16] $ZnSnO_3$,[17] PZT,[18,19] PMN−PT,[20] and $BaTiO_3$[14,21,22] have been widely examined. Among them, PZT-based PNGs have more power generation due to their high piezoelectric coefficient (d_{33}), but face global restriction due to lead toxicity causing human health problems, bioincompatibility, and environmental pollution. Therefore, the development of environmentally friendly and biocompatible PNGs based on lead-free piezoelectric ceramics has received increasingly significant attention.[23] $BaTiO_3$-based ceramics are alternative candidate for the development of PNGs compared to PZT-based ceramics due to the following merits: a lower piezoelectric coefficient but smaller dielectric constant (which could possibly be improved by doping foreign atoms)[24,25] and biocompatibility for implantable biological devices.[21,23]

In this paper, we first demonstrate the flexibility of the PNG based on a high performance composite film composed of BTZO (x = 0, 0.05, 0.1, 0.15, and 0.2) nanocubes and a poly(vinylidene fluoride) (PVDF) polymer matrix. High purity bulk $BaTiO_3$ nanocubes (without a change in the tetragonal structure) have been modified by the substitution of a Zr^{4+} atom (0.72 Å) in place of the Ti^{4+} (0.605 Å) site using the molten salt method. The substitution of a Zr^{4+} atom in the Ti^{4+}

Received: February 28, 2015
Accepted: April 22, 2015
Published: April 22, 2015

DOI: 10.1021/acsami.5b01760
ACS Appl. Mater. Interfaces 2015, 7, 9831−9840

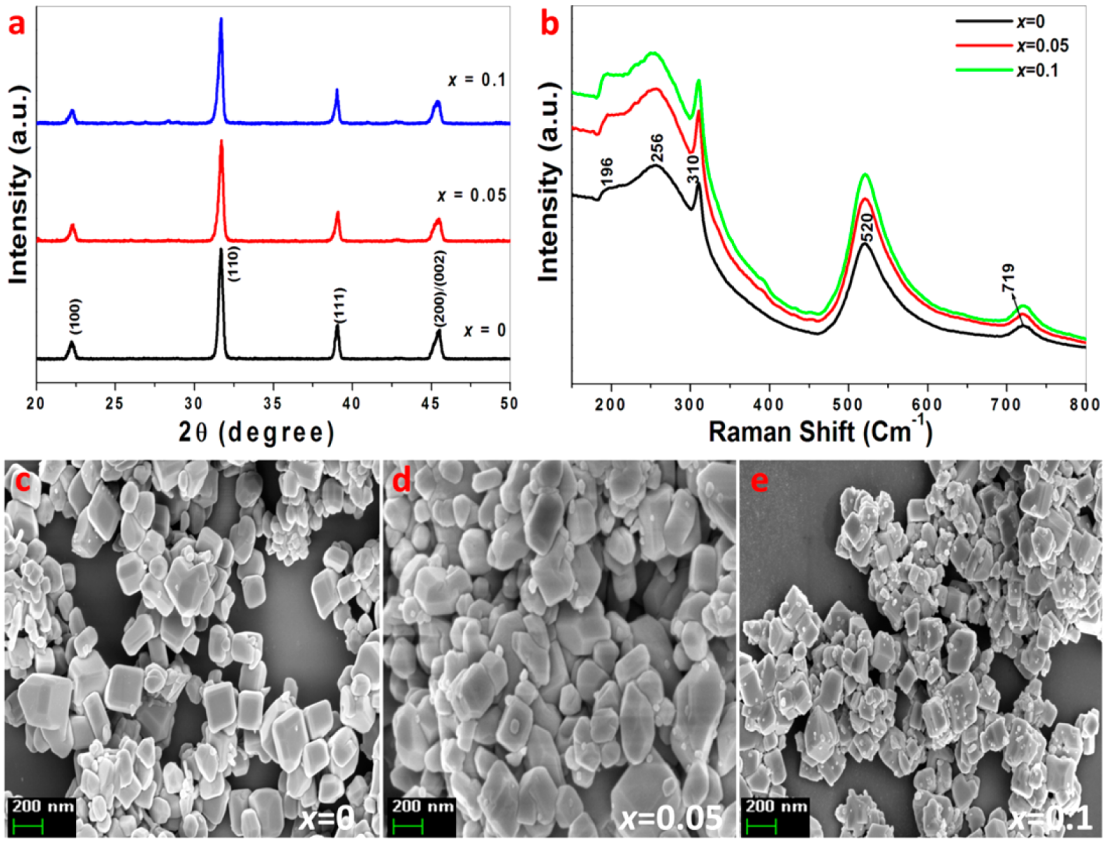

Figure 1. Structural and surface morphology of $BaTi_{(1-x)}Zr_xO_3$ (x = 0, 0.05, and 0.1) nanocubes processed by the molten salt method. (a) X-ray diffraction patterns of highly crystalline BTZO nanocubes after calcination. (b) Typical Raman spectrum for BTZO nanocubes indicating the formation of a tetragonal crystal structure. (c–e) FE-SEM images showing the crystalline surface morphology of BTZO nanocubes on a 200 nm scale.

site enhances the piezoelectric coefficient (d_{33}) from 100 pC/N ($BaTiO_3$)[26−28] to 174−236 pC/N ($BaTi_{(1-x)}Zr_xO_3$)[29,30] and electromechanical conversion efficiency, which is better for harvesting energy. The electrical characterization (open-circuit voltage and short circuit current) of as-prepared $BaTi_{(1-x)}Zr_xO_3$/PVDF nanogenerators was studied, demonstrating a capacity to light five green LEDs simultaneously without any storage device through successfully harvesting of biomechanical energy. The maximum open-circuit voltage and short circuit current for $BaTi_{0.9}Zr_{0.1}O_3$ nanocube/PVDF-based PNG reached 11.9 V and 1.36 μA, respectively, which are greater than the $BaTiO_3$ nanocube/PVDF output of 7.99 V and 1.01 μA. In addition, we demonstrated that the $BaTi_{0.9}Zr_{0.1}O_3$/PVDF-based PNG acts as an active sensor. The electrical outputs of this PNG can be examined to estimate their input water velocity (inertial forces) flowing through the outlet pipe. Recently, a few reports has been published describing piezoelectric NGs as active sensors for heart-pulse,[31] tire pressure,[32] cantilever vibration,[33] and wind-velocity detection[2] measurements. This study will expand the choice of materials for PNGs and demonstrate that the utilization of PNG as an active sensor has more advantages, including being pollution free and having a low maintenance cost, high operating temperature up to 120 °C, and long lifetime.

EXPERIMENTAL DETAILS

Synthesis of $BaTi_{(1-x)}Zr_xO_3$ Nanocubes. The stiochiometric compositions $BaTi_{(1-x)}Zr_xO_3$ (x =0, 0.05, 0.1, 0.15, and 0.2) were synthesized by the molten salt method,[34,35] which is schematically shown in Figure S1 (in the Supporting Information (SI)). Commercial powders of $BaCO_3$ (99.95%), TiO_2 (98%), and ZrO_2 (99%) were selected as starting materials. The raw materials were weighed according to their stoichiometric ratio and mixed with a eutectic mixture of 50:50 mol % NaCl and KCl flux and an extra salt, 25% mol Na_2SO_4, acting as the reaction medium. To obtain a homogeneous powder, the raw materials were mixed by hand-grinding in a mortar and pestle in ethanol solution for 30 min. The as-synthesized mixture was placed into a combustion boat and heated at 750 °C for 3 h in a furnace. The heating rate is 2.5 °C/min, and the product was removed from the furnace for natural cooling after the reaction. Finally, the as-synthesized product was washed with hot deionized water several times until no chloride ions were detected by silver nitrate solution to ensure that the salt residue was exhaustively removed, and it was then dried at 60 °C overnight. This approach allows the low firing temperature (750 °C/3 h) to be enriched in its morphology as compared to BTZO-derived with a high firing temperature (>1100 °C/2 h) by the solid state reaction process.[29,36,37]

Hybrid (or Composite) Film and Nanogenerator Fabrication. A schematic representation of the composite film using the ultrasonication process is shown in Figure S5 (in the SI). A total of 1g of PVDF (Sigma-Aldrich) was dissolved in a mixture of 5 mL of *N*,*N*-dimethylformamide (DMF) and 3 mL of acetone, and a homogeneous solution was obtained by the sonication process using a probe sonicator for 60 min. Next, 25 wt % of $BaTi_{(1-x)}Zr_xO_3$ (x = 0, 0.05, 0.1, 0.15, and 0.2) nanocubes was mixed with the prepared solution and sonicated for 1 h using a probe sonicator. The final solution was poured into a Petri dish and dried in a hot-air oven at 60 °C overnight. The dried film was peeled off of the Petri dish and modified according to the required dimensions (2.5 cm × 2.5 cm) of a nanogenerator (NG). The NG was fabricated by coating Al electrodes on top and bottom of the hybrid film through the thermal evaporation

DOI: 10.1021/acsami.5b01760
ACS Appl. Mater. Interfaces 2015, 7, 9831−9840

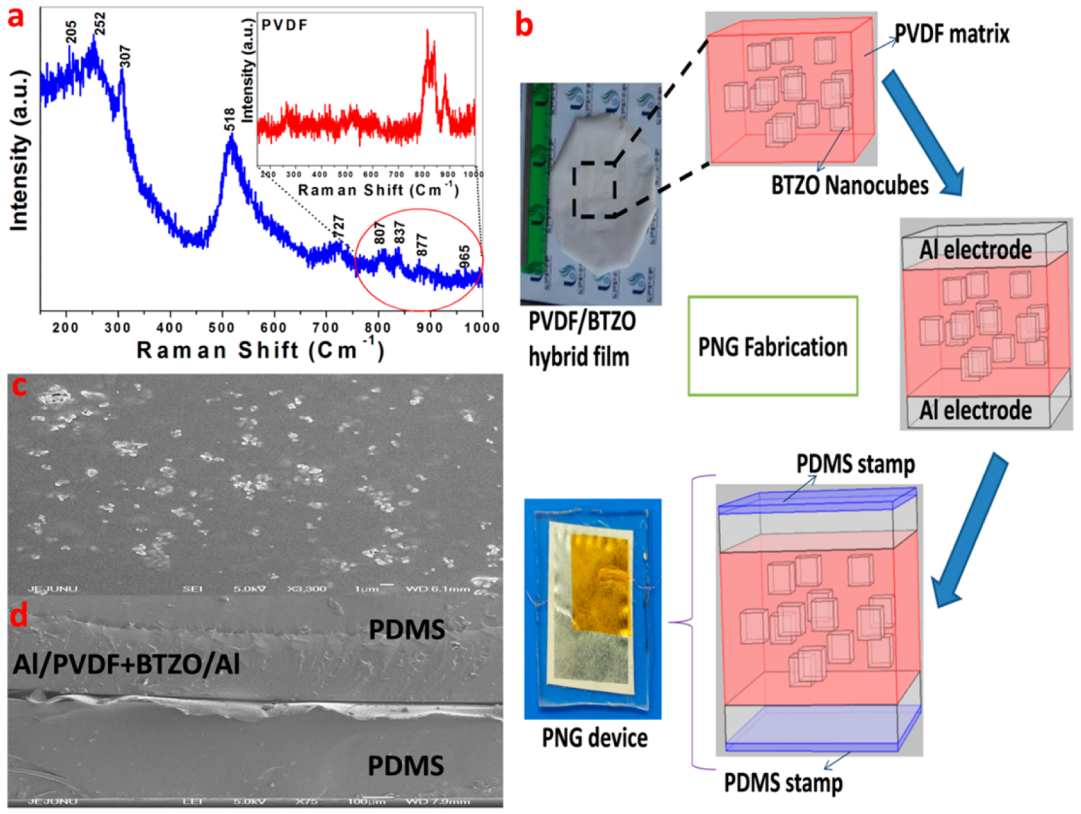

Figure 2. (a) Typical Raman spectrum of a $BaTi_{0.9}Zr_{0.1}O_3$/PVDF piezoelectric composite film by the ultrasonication probe method. The inset shows the Raman spectrum of the PVDF polymer matrix. (b) Schematic diagram of various key steps during the fabrication of a $BaTi_{0.9}Zr_{0.1}O_3$/PVDF PNG device. (c) FE-SEM image of $BaTi_{0.9}Zr_{0.1}O_3$/PVDF hybrid film showing its well dispersed $BaTi_{0.9}Zr_{0.1}O_3$ nanocubes into the polar β-phase of the PVDF polymer matrix. (d) A magnified cross-sectional FE-SEM image of the PNG device showing its Al-coated top and bottom surface of the hybrid film covered with PDMS stamps.

technique. Electrical connections were established by Cu wires attached with silver paste on top and bottom of the Al-coated hybrid film. Finally, polydimethylsiloxane (PDMS) was used as a packaging layer for the NG to protect the device from external conditions, such as mechanical stress, temperature, and humidity. Before electrical characterization, the NG was poled at ambient temperature by applying a high voltage of 8 kV for 24 h. To demonstrate the self-powered sensor, the PNG was kept normal to the water flow with a fixed rigid support covered with polyethylene (PE) material.

Measurement System. The phase formation of as-synthesized BTZO nanocubes were obtained with an X-ray diffractometer (XRD, Rigaku) operated at 40 kV and a current of 40 mA patterns recorded using Cu Kα radiation (2θ range from 20° to 50°) at room temperature. Raman spectra for all samples were recorded from 150 to 800 cm^{-1} with an excitation source of 514 nm using a high throughput single stage spectrometer (LabRAM HR Evaluation, Japan). The morphological analysis of BTZO solid compositions and hybrid films (BTZO/PVDF) was performed by a field emission-scanning electron microscope (FE-SEM Zeiss Supra-55vp). The electrical outputs (i.e., open circuit voltage (V_{oc}) and short circuit current (I_{sc}) of NG) were recorded by a nanovoltmeter (Keithley 2182A) and picoammeter (Keithley 6485), respectively. Measurement of the PNG's output was triggered by an electrodynamic shaker (ET-126) with different frequencies (3, 11, and 21 Hz) at a fixed input amplitude of 5 V.

RESULTS AND DISCUSSION

A large number of high-quality BTZO nanocubes were synthesized through the molten salt method. The complete preparation process of BTZO nanocubes is depicted in the Experimental Details section. Figure 1a shows the XRD patterns of as-synthesized BTZO (x = 0, 0.05, and 0.1) piezoelectric nanocubes, which reveals a single-phase perovskite structure, indicating that Zr^{4+} may have entirely diffused into the $BaTiO_3$ lattice to form a solid solution in which the Zr^{4+} (0.72 Å) atom substituted in the Ti^{4+} (0.605 Å) site. The major XRD peaks of BTZO (x = 0, 0.05, and 0.1) were ascribed to tetragonal crystal structure,[34] but the increase in Zr^{4+} content (i.e., x > 0.1) results in minor intermediate phases with tetragonal crystal structure (Figure S2a in the SI), which indicates a doping limit up to x = 0.1 using the molten salt method. The tetragonal structure (ICDD-98-001-3771) is observed by splitting of the diffraction peak at 45°, indexed as (002)/(200).[34,38] BTZO nanocubes are well-crystallized perovskite structures, but the tetragonal distortion of BTZO, $\delta = (c - a)/a$, is up to 1% in bulk materials and is typically identified by the line broadening effect[22] of the XRD pattern. Thus, the detailed dynamic symmetry and structural information was monitored by Raman spectroscopy as shown in Figure 1b. Mostly, $BaTiO_3$ with a cubic structure does not have Raman active modes, but the tetragonal structure does have active modes due to its non-centrosymmetric property. The Raman spectra of $BaTiO_3$ nanocubes are identified at 196 cm^{-1} [A_1(TO), E(LO)], 256 cm^{-1} [A_1(TO)], 310 cm^{-1} [B_1(TO+LO), E], 520 cm^{-1} [A_1(TO), E], and 720 cm^{-1} [A_1(LO), E], all of which are subject to the tetragonal phase of $BaTiO_3$.[14,22,39,40] As the Zr^{4+} concentration was increased up to x = 0.15, there was not much of a considerable peak shift. When x = 0.2, the Raman peak at 256 cm^{-1} appears to be very weak, which indicates the existence of a rhombohedral tetragonal phase[24] (Figure S2b in the SI). The Raman shift

DOI: 10.1021/acsami.5b01760
ACS Appl. Mater. Interfaces 2015, 7, 9831−9840

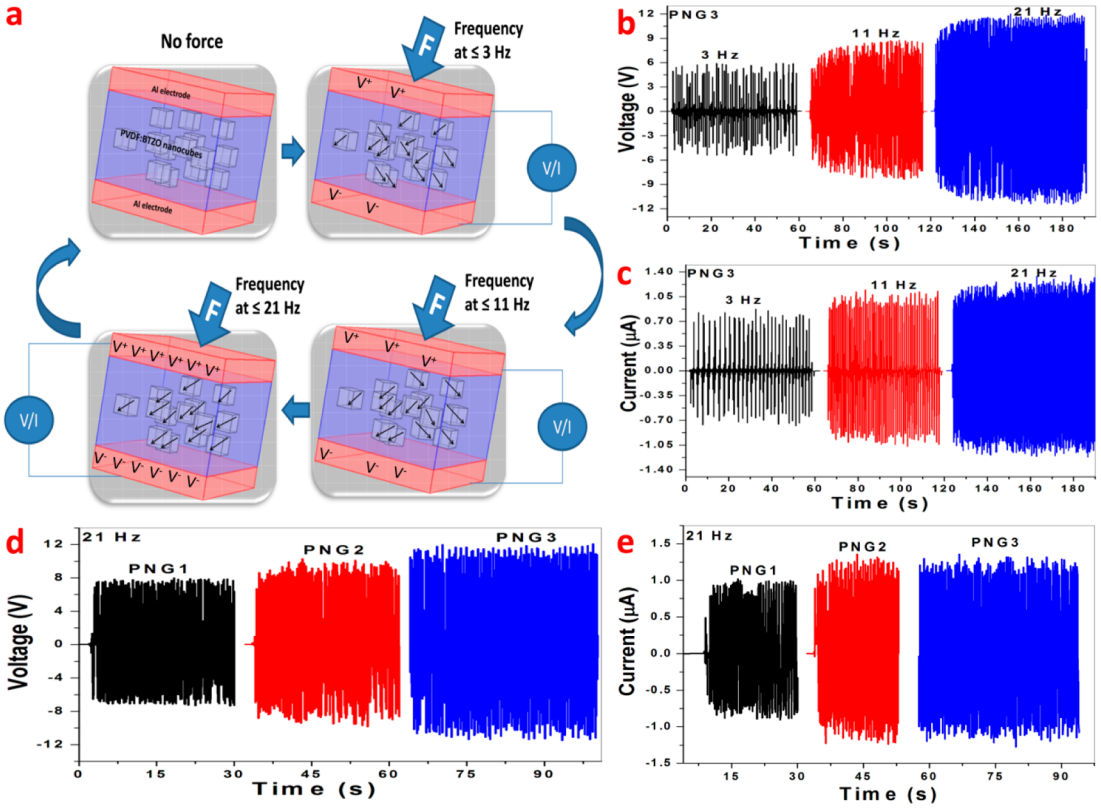

Figure 3. (a) Proposed mechanism of the BTZO nanocube/PVDF-based PNG. No output signal is observed in the absence of an external mechanical load. The electrical output signal is observed for PNGs under an external mechanical load (11 N) with respect to cyclic frequency (3, 11, and 21 Hz) of the electrodynamic shaker. (b, c) Output voltage and current of PNG3 as a function of the cyclic frequency of the mechanical load. (d, e) Comparison of the electrical output voltage and current of PNG1, PNG2, and PNG3 upon the application of a mechanical load at 21 Hz cyclic frequency.

and XRD pattern indicates the presence of non-centrosymmetric regions formed from local off-centering of the titanium (zirconium) atoms. The FT-IR spectra shows that Zr^{4+} additives will directly affect the stretching and bending vibration of the crystal lattice ($BaTiO_3$) as shown Figure S3a in the SI. Generally, the most important peak for barium titanate corresponds to the wavelength range between 530−600 cm^{-1}. This peak is due to the vibration of the bond between titanium and oxygen (Ti−O bond). In this study, $BaTiO_3$ nanocubes were prepared via the molten salt method with a lattice absorption peak at 552 cm^{-1}, which is shifted toward the lower wavelength side, when increasing the Zr^{4+} substitution into the Ti^{4+} site as shown in Figure S3b in the SI. The field emission scanning electron micrograph (FE-SEM) images depicted in Figure 1c−e reveal the high purity of BTZO nanocubes (200 nm scale). As the amount of Zr^{4+} is increased in $BaTiO_3$, small sized grains other than nanocubes are formed, and at the same time, the shape of the nanocubes themselves are modified (Figure S4a and b in the SI). Tetragonal BTZO exhibits ferroelectric properties as a result of the lattice distortion of the Ti ion coordinating with the octahedral oxygen groups and substitution of the Zr ion in the Ti site.[29,38,39] Figure 2a shows that the Raman shift of the $BaTi_{0.9}Zr_{0.1}O_3$/PVDF hybrid film replicates the well processed $BaTi_{0.9}Zr_{0.1}O_3$ nanocubes in the PVDF polymer matrix. This indicates no change in the tetragonal structural modes at 307 and 727 cm^{-1} of BTZO nanocubes into the PVDF matrix (sonication process for 1 h and curing at 60 °C overnight). The inset shows the Raman spectrum of the polarized PVDF phase (Figure 2a). X-ray diffraction is used to identify the characteristic phase of the PVDF matrix and indicates that the diffraction peak at 20.36° corresponds to the polar β phase[41] (Figure S6a in the SI). In the sonication process, the sound energy plays a key role in obtaining a homogeneous distribution of BTZO nanocubes in the PVDF matrix and removal of dissolved gases from the liquid by breaking intermolecular interactions. Figure 2b demonstrates a schematic approach to generating BTZO/PVDF PNGs, and the inset shows an optical image of a final processed hybrid film ($BaTi_{0.9}Zr_{0.1}O_3$/PVDF) and its device. Al electrodes were coated on top and bottom of the hybrid film via a thermal evaporator. Silver paste is used to attach the Cu wires with electrodes for external connections and are covered with a small piece of kapton. Later, the dipoles of the device are aligned at an ambient temperature by applying an electric field of 8 kV for 24 h. All of the other hybrid films are developed using the same kind of methodology. Lastly, a fine thin layer of PDMS is used to package the device to protect from environmental stimuli, such as temperature, mechanical force, and humidity. The surface morphology of the hybrid film and a magnified image of the cross-sectional view of the PNG as analyzed by FE-SEM are shown in Figure 2c and d, respectively.

The working mechanism of the hybrid film-based PNGs was investigated. The working principle of the PNG is based on the piezoelectric properties of BTZO nanocubes and the creation of an inner piezoelectric field inside the BTZO nanocubes in a PVDF matrix under an applied mechanical load with cyclic frequency. Because Zr^{4+} ions substituting in the Ti^{4+} site will

DOI: 10.1021/acsami.5b01760
ACS Appl. Mater. Interfaces 2015, 7, 9831−9840

enhance (or reduce) the piezoelectric coefficient electromechanical coupling factor, which is purely dependent on the amount of Zr doping.[29] If Zr ≤ 0.1, it has normal ferroelectric properties with an enhanced piezoelectric coefficient (200−300 pC/N,[29,30,42] vs 420 pC/N[43] at 100 h sintering) as compared to $BaTiO_3$ (bulk). When the Zr concentration is >0.1, relaxor ferroelectric behavior with smaller piezoelectricity is observed[29,30,42,43]. In the present case, the piezoelectric potential generation is mainly dependent upon the cyclic frequency of the load as shown in Figure 3a. In PNGs, no output signal is observed in the absence of an external mechanical load due to the random orientation of the dipoles existing in the hybrid film (BTZO/PVDF), which results in zero net dipole momentum (Figure S7 in the SI). An external compressive load (11 N) with a low cyclic frequency of 3 Hz is applied across the PNGs, resulting in low piezoelectric potential being generated across the electrodes, which may be due to either capacitance or the initiation of piezoelectric behavior. However, with the application of the same load with high cyclic frequency (3−11 Hz reaching 21 Hz), the piezoelectric potential reaches a maximum (Figure 3b and c), which indicates that the orientation of the electric dipoles in the hybrid film are in a particular direction due to the stress-induced poling effect.

In the present work, we correlated the generated piezoelectric potentials of $BaTiO_3$/PVDF (abbreviated as PNG1) and $BaTi_{(1-x)}Zr_xO_3$ (x = 0.05 and 0.1)/PVDF-based PNGs (abbreviated as PNG2, PNG3) mechanically triggered by an electrodynamic shaker providing a dynamic impact with controlled frequency, speed, and force. We observed that the voltage and current of the PNGs are affected by the cycling frequency (3−21 Hz) at a fixed input amplitude (or load) of the shaker. At the first instance, the electrical output of PNG1 was achieved at 3.42 V and 0.44 μA by cyclic pushing-releasing frequency at 3 Hz with a fixed load of the shaker (Figure S8a and b in the SI). During the pushing process, the dipoles are oriented perpendicular to the plane of the film. This results in accumulation of opposite charge carriers on the top and bottom surface of the $BaTiO_3$/PVDF film, which is collected by external electronic circuitry.[22] Once the external stress is released, the piezoelectric potential vanishes, and the charge carriers move back to their original state. When the cyclic frequency of the load increases from 3 to 21 Hz, the output varies from 3.42 V and 0.44 μA to 7.99 V and 1.01 μA (Figure 8a and b in the SI), indicating cyclic frequency-dependent behavior of the hybrid $BaTiO_3$/PVDF film.

The generated piezoelectric potential distribution is mainly due to the stress-induced transient flow of free charge carriers,[14,22,44] is aroused by the active β-phase of PVDF (positive and negative charge carriers displaced in a VDF molecule), and is due to non-centrosymmetric $BaTiO_3$, where the atoms are displaced from their equilibrium positions. It is well-known that the β-phase of PVDF has a small piezoelectric potential generation[16,45] as compared to other piezoelectric materials like PZT,[18] $BaTiO_3$,[14] and KNLN.[46] Here, PVDF is utilized in two ways; it works as a substrate to support the whole structure, with the flexible nature of PVDF reducing the processing time to make the device dimensions for specific applications, and its piezoelectric coefficient is negative,[16] whereas that for $BaTiO_3$ is positive. Thus, through the proper poling direction and compressive force, it may be possible to enhance the electric potential difference across the top and bottom of the Al electrodes. However, analysis of the contribution of poled PVDF-based PNG (without BTZO nanocubes) under a cyclic frequency of 21 Hz with same mechanical load shows less output (Figure S9 in the SI) than that of the hybrid film (BTZO/PVDF-based PNG) (Figure 3d and e). Similarly, analysis of the unpoled PVDF-based PNG shows very low output (Figure S10 in the SI), indicating that the potential generation is based purely on the piezoelectric effect (and not a triboelectric effect). The generated piezoelectric potential, dependent on the piezoelectric coefficient, can be expressed as[47,48]

$$V_{OC} = g_{33}\sigma Yt \tag{1}$$

where σ is the strain in the perpendicular direction, g_{33} is the piezoelectric voltage constant ($g_{33} = d_{33}/(\varepsilon_0 K)$, in which d_{33} is the piezoelectric charge constant, ε_0 is the permittivity of free space, and K is the dielectric constant or relative permittivity), Y is Young's modulus, and t is the thickness of the device. According to eq 1, factors that will improve the generated output voltage of the device are as follows: high d_{33}, low relative permittivity (K), and high elastic modulus. The $BaTiO_3$ nanocubes embedded with polymer matrix will improve the elastic modulus and reduce the dielectric constant.[21] However, the internal resistance of the piezoelectric film will change according to the driving frequency and mechanical load. At low driving frequency of the mechanical load, the centers of both positive and negative charge carriers may not totally separate, resulting in a smaller piezoelectric potential. Upon increasing the driving frequency of the mechanical load, the centers of both positive and negative charge carrier separations reach a maximum value (i.e., the maximum number of dipoles will orient in one direction), corresponding to the generation of higher piezoelectric potentials in the nanogenerators as shown in Figure 3b and c. Recently, different cycling-frequency-dependent electrical output of PNGs was examined well. According to the fundamental piezoelectric theory,[16] the short circuit current can be written as

$$I = d_{33}YA\varepsilon \tag{2}$$

where I is the generated current, d_{33} is the piezoelectric coefficient, E is Young's modulus, A is the cross-sectional area, and ε is the applied strain. The energy conversion efficiency of the PNGs is the ratio of generated electrical energy and applied mechanical energy. Subsequently, we characterized the electrical output of the PNG based on the compositional dependence of the nanomaterials (different Zr^{4+} ratios doped to $BaTiO_3$ nanocubes in the Ti^{4+} site) embedded in a PVDF matrix under the periodic motion of mechanical stress. The result of all of the PNGs indicates cyclic frequency-dependent behavior at a fixed load. The amplitude of the output voltage and current generated from PNG2 are 10.3 V and 1.35 μA at 21 Hz cyclic frequency (load = 11 N) after the doping of 5% mole content (Zr^{4+}) to $BaTiO_3$ nanocubes. Similarly, the voltage and current for PNG3 are 11.9 V and 1.35 μA after the doping of 10% mole content (Zr^{4+}) to $BaTiO_3$ as shown in Figure 3d and e, which clearly shows that Zr-doped PNGs have an enhanced electrical output compared to that of undoped $BaTiO_3$-based PNGs. This may be due to enhancement of the piezoelectric coefficient (d_{33}) of the hybrid film. The increment in d_{33} is due to the coexistence of polymorphic phase boundaries,[29] such as orthorhombic ($Amm2$) + tetragonal ($P4mm$) to orthorhombic ($Amm2$) + rhombohedral ($R3m$) phases. A recent study shows the average piezoelectric response (d_{33} = 285−290 pC/cm^2) in the composition range $0.02 \le x \le 0.08$ ($BaTi_{1-x}Zr_xO_3$) does not vary significantly with the composition, which is greater

DOI: 10.1021/acsami.5b01760
ACS Appl. Mater. Interfaces 2015, 7, 9831−9840

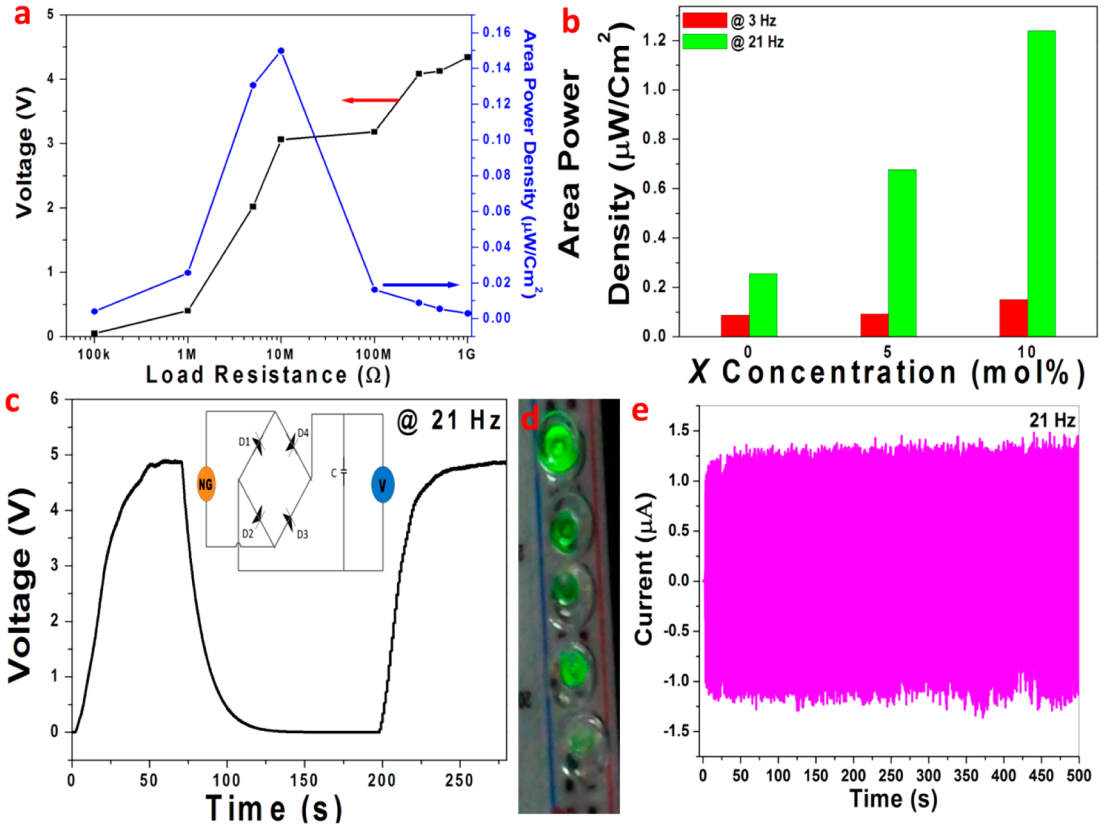

Figure 4. (a) At a cyclic frequency of 3 Hz with a fixed load, the output peak voltage and area power density dependence on the load resistance of the PNG3 device are presented. (b) Comparison of area power density of PNG1, PNG2, and PNG3 upon cyclic frequency of 3 and 21 Hz of mechanical load at a maximum load resistance of 10 MΩ, showing the role of Zr^{4+} (mol %) substitution into $BaTiO_3$. (c) Voltage across a storage capacitor (1 μF) while being charged by PNG3 with the full wave bridge rectifier at 21 Hz. (d) Five commercial green LEDs can be lit by the rectified piezoelectric potential from PNG3 without any storage device. (e) Output current of PNG3 under 21 Hz frequency, demonstrating the stability of the nanogenerator.

than the $BaTiO_3$ (bulk) piezoelectric coefficient (d_{33} = 150 pC/cm^2).[29] Phase coexistence may be possible due to the higher ionic radius of Zr^{4+} ion substituted at the Ti^{4+} ion site, which in turn creates lattice distortion by the TiO_6 octahedron of $BaTiO_3$. According to eq 1, V_{OC} is directly proportional to d_{33}, and the electrical output voltage increased from 0% to 10% of Zr^{4+} of $BaTiO_3$ along with the PVDF matrix, indicating the d_{33} increment behavior. As we increased the doping concentration to >10% of Zr^{4+} ion into the $BaTiO_3$/PVDF-based PNG, a lower electrical output results compared to that of the pure $BaTiO_3$-based PNG (Figure S11 in the SI) due to the smaller piezoelectric coefficient.[29] The PNGs instantaneous power delivered to the load could be estimated from the following equation.[19,49]

$$P = \frac{1}{T}\int \frac{V^2(t)}{R}\,dt \tag{3}$$

where P is the power and V is the real-time peak voltage across the load resistance R, and T is the period of mechanical load. The PNG device is a planar structure; therefore, the power scales will depend on the active area (A) of the device. The voltage of PNG3 was measured by connecting output terminals across the variable resistor (R) and, correspondingly, the instantaneous area power density evaluated by using eq 3 divided by the area (A) of PNG (i.e., $P_A = P/A$). The power is maximum (0.14 μW/Cm^2) for PNG3 across the load resistance (10 MΩ) at 3 Hz cyclic frequency of the load (11 N) as shown in Figure 4a, which indicates that the maximum optimum load resistance (or equivalent) of the PNG3 device is 10 MΩ. Similarly, the output voltages of all of the PNGs were evaluated across the resistance (10 MΩ) at 3 and 21 Hz cyclic frequency and fixed load (11 N) as shown in Figure 4b, which clearly shows that the Zr^{4+}-doped $BaTiO_3$/PVDF-based device has a higher power density than that of pure $BaTiO_3$. The detailed equivalent resistance of a PNG can be evaluated as[4]

$$R_P = \frac{d}{A\varepsilon_p f} \tag{4}$$

where f is the frequency of the external force, and d, A, and ε_p are the thickness, area, and permittivity of the hybrid film (BTZO/PVDF), respectively. Besides the instantaneous area power density, the charging ability of the PNG was also measured and analyzed. The experiment was carried at 21 Hz cyclic frequency with an external force of 11 N applied to PNG3. The generated output voltage was rectified to continuously charge a 1 μF capacitor; the output voltage reaches ~5 V in ≤50 s (Figure 4c). Next, five commercial green LEDs lit up with generated piezoelectric potential for all devices using the bridge rectifier circuit without any storage devices (Figure 4d). A durability test was conducted to confirm the mechanical stability of the PNG at 21 Hz cyclic frequency with an applied load of 11 N as shown in Figure 4e. The current of PNG3 did not change significantly during the 500 s interval. Next, to estimate the sensitivity of the PNG, the experiment

DOI: 10.1021/acsami.5b01760
ACS Appl. Mater. Interfaces 2015, 7, 9831−9840

was conducted by successive tapping with a right-hand finger (in a gentle manner), and the rectified electrical response for all devices is shown in Figure S12 (in the SI). The generated piezoelectric potential is up to 4 V driven by biomechanical force, which is sufficient for lighting the commercial LEDs. This indicates that our proposed energy harvesting device is a potential candidate for remote area applications in which battery energy is necessary. A polarity test was conducted to confirm the piezoelectric output driven by a biomechanical force as shown in Figure S12d (in the SI). The results described above demonstrate that alternating energy generated from PNG devices is stored in capacitors (or without) and is subsequently useful for self-powered sensors, implantable devices, and low power electronic applications. In this work, the PVDF/BTZO nanocube weight ratio (1:0.25 g/g) was fixed for simplicity. We also observed that the PNG performance can be varied by changing the weight ratio of PVDF/BTZO, external mechanical stress, electric poling, and the piezoelectric coefficient of the hybrid film. However, the proposed PNGs output performance is better, and is even higher output than that described by a few published nanogenerator reports, based on individual $BaTiO_3$, PVDF, and composite structures as shown in Table 1. The process used to fabricate the PNGs is

Table 1. Comparison of the Proposed Device Performance with Other Reported Organic and Composite Piezoelectric Nanogenerators

material	microstructure	VOC[a] (V)	ISC[b] (nA)	refs
PVDF/$BaTiO_3$	nanocubes	7.99 @ 11 N load	1010 @ 11 N load	present work
PVDF/$Ba(Ti_{0.95}Zr_{0.05})O_3$	nanocubes	10.03 @ 11 N load	1350 @ 11 N load	present work
PVDF/$Ba(Ti_{0.9}Zr_{0.1})O_3$	nanocubes	11.99 @ 11 N load	1360 @ 11 N load	present work
$BaTiO_3$/PDMS	nanotubes	5.5	350	22
$BaTiO_3$/MW-CNT/PDMS	round shape	3.2	350	40
$BaTiO_3$ thin film		1	26	50
PAA/13 nm OA-$BaTiO_3$	cubic-like	1.8	700	39
virus-template BTO/PDMS		6	300	51
$BaTiO_3$	single nanowire	0.021	1.3	21
BZT-xBCT	nanowires	3.25	55	52
PVDF	single fibers	0.03	3	16
PVDF	fibers	0.076	39	45
PVDF-TrFE		7	58	53

[a]Open circuit voltage of the piezoelectric nanogenerator. [b]Short circuit current of the piezoelectric nanogenerator.

relatively simple, cost-effective, and amenable to large-scale production. This type of PNG has many advantages compared to those of lead-based PNGs due to its sensing capability, biocompatibility,[23] nontoxicity,[25,46] and eco-friendly behavior.[47]

A flexible PNG can be used as an active sensor, capable of measuring different water velocities at an outlet pipe due to its high sensitivity and conformability. As a demonstration, a PNG with a size of 2.5 cm × 2.5 cm was attached to a fixed, rigid support and placed perpendicular to the water flow as shown in Figure S13a in the SI (control experiment photograph). To avoid direct surface contact between water and the PNG, a polyethylene (PE) cover was attached to the surface of the PNG. The electrical response of PNG3 at different water velocities of the outlet pipe is shown in Figure 5a and b. The PNG was driven by a rotating faucet at a fixed position with two conditions, water ON and water OFF, over periodic time intervals (inset, Figure 5a and b). At a water velocity of 31.43 m/s, the average output voltage and current of PNG3 achieved were 26 mV and 8 nA, respectively, during the water ON condition; during the water OFF condition, the voltage and current were 80 mV and 10 nA, respectively. Upon increasing the water velocity from 31.43 to 78.6 and to 125.7 m/s, the corresponding output voltages and currents reached 213 and 466 mV and 19 and 34 nA, respectively, during the water ON condition.

Here, the mechanism involved during the water ON and OFF conditions is similar to the force acting on PNG by pushing and releasing load with periodic manner. During the water ON condition, the induced charges move across the top and bottom surface of the PNG, resulting in piezoelectric potentials with different polarities that were generated in the same plane of the NG. During the water OFF condition, the induced charges move back to their original sites. To identify the water velocity at the outlet pipe, a control experiment was performed by rotating a faucet to estimate the amount water falling per second (ml/s). The water flow rate (Q) in the pipe as a function of faucet rotation (i.e., position) can be approximated as $Q = (V/A)$, where V is the velocity at the outlet and A is the area of the circular plastic pipe shown in Figure 5c. To maintain constant pressure at different water velocities, a water tank was filled with a fixed amount of water having a height (h) and pressure (p = 1 atm). The detailed experimental procedure and working principles are given in the SI. The average maximum peak power of the PNG under the water ON condition as a function of different water velocities is shown in Figure 5d. The average maximum peak power (w_e) generated by PNG under the impact of different water velocities can be evaluated as[16]

$$w_e = \int VI\, dt \tag{5}$$

where V and I are the average measured output voltage and current, respectively, of PNG. The achieved average maximum power is 0.2 nW for 31.43 m/s water velocity and increased up to 15.8 nW at 125.7 m/s. Similarly, the achieved average maximum peak power during the water OFF condition was evaluated and is shown in Figure 5d, which is quite smaller than that of the ON condition. At the water OFF condition, a small amount of water droplets settled on the PNG device, which in turn restrict the transient charge carrier motion. These experiments reveal that energy can be harvested by a piezoelectric composite via natural water motion, such as home water waste, seawater, rivers, and even rain. This can also be useful as an active sensor in various fields, such as pump monitoring, process control, and HVAC (heating, ventilating, and air conditioning).

CONCLUSIONS

In summary, flexible PNGs were fabricated based on hybrid films composed of BTZO nanocubes and a PVDF polymer matrix using an ultrasonication probe process. Next, it was successfully demonstrated that PNGs functionality can be useful as a self-powered sensor where battery energy is required. Enriched crystalline BTZO nanocubes were success-

DOI: 10.1021/acsami.5b01760
ACS Appl. Mater. Interfaces 2015, 7, 9831−9840

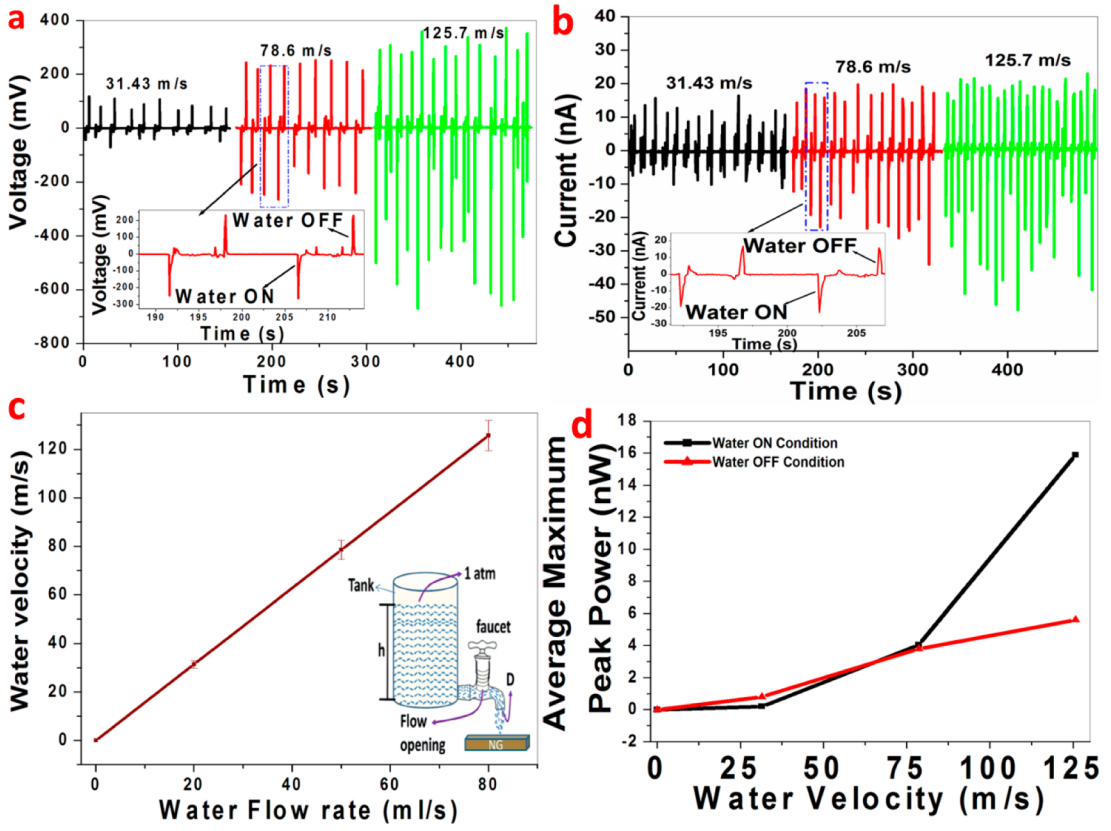

Figure 5. Demonstration of PNG3 as a self-powered sensor to measure different water velocities flowing through the outlet pipe. (a, b) Open circuit voltage and short circuit current of PNG3 at water velocities of 31.43, 78.6, and 125.7 m/s. The insets of (a, b) show output generated under water ON and OFF conditions. (c) Linear relationship between the water velocities (m/s) at the outlet pipe and flow rate (ml/s); the inset shows a schematic diagram of the control experiment. (d) The generated average maximum output peak power ($W = PI$) obtained at different velocities under the water ON condition. The inset shows the obtained peak power under water the OFF condition.

fully synthesized using a low processing temperature (750 °C/3 h) (i.e., molten salt approach) as compared to the solid state reaction method (>1100 °C/2 h). The Zr^{4+}-doped (<10% mole content) PNG has a piezoelectric output power generation of 11.9 V and 1.36 μA as compared to the BTO/PVDF-based PNG of 7.99 V and 1.01 μA, respectively. We observed that the PNG performance depends on the mechanical load, electric poling, and the piezoelectric coefficient (i.e., is indirectly dependent on the BTZO/PVDF weight ratios). This study demonstrates that the PNG electrical output depends on the compositional fluctuation and cyclic frequency of the mechanical load. In addition, the PNG output power generated can be stored in capacitors, which could be useful for driving commercial LEDs, low power electronic devices, and self-powered sensors. By a stability test using a cyclic pushing instrument, superb reproducibility and durability of the PNGs was confirmed. Then, we successfully demonstrated the application of the PNG as a self-powered sensor to measure water velocities at an outlet pipe. The PNG-based self-powered sensor can be operated at a high fluid operating temperature (up to 120 °C) and over high pressure ranges for such a small device size. The reported PNG results are also comparable to or higher than many other lead-free-based PNG devices, which are valuable for active sensors, portable devices, pump monitoring, and process control fields.

■ ASSOCIATED CONTENT

Supporting Information

(1) Process flowchart for $BaTi_{1-x}Zr_xO_3$ nanocubes via the molten salt method. (2a, b) XRD pattern and Raman spectra of $BaTi_{1-x}Zr_xO_3$ nanomaterials for x = 0.15 and 0.2, confirming a polymorphic nature at room temperature. (3a, b) FTIR spectra and lattice absorption shift of $BaTi_{(1-x)}Zr_xO_3$ (x = 0, 0.05, 0.1, 0.15, and 0.2) nanocubes. (4a, b) Surface morphology of BTZO (x = 0.15 and 0.2) nanomaterials on a 200 nm scale. (5) Schematic diagram for the PVDF/BTZO hybrid piezoelectric film process. (6a, b) XRD patterns of a processed PVDF film by ultrasonication to confirm the existence of the β-phase, and it is FESEM on a 10 μm scale. (7) Electrical output signal of PNG3 during external mechanical loading and no load conditions at 3 Hz. (8) Electrical outputs of PNG1 and PNG2 under cyclic frequencies of 3, 11, and 21 Hz at a fixed load of 11 N. (9) Electrical outputs (voltage and current) of PVDF-based PNG3 (poled PVDF sample) upon 21 Hz at a fixed load of 11 N. (10) Electrical response of PVDF-based PNG (without poling) upon cyclic frequencies of 3, 11, and 21 Hz at a constant mechanical load (11 N). (11) Electrical output of PNG4 ($BaTi_{0.85}Zr_{0.15}O_3$/PVDF) and PNG5 ($BaTi_{0.80}Zr_{0.2}O_3$/PVDF) devices under cyclic pushing and releasing frequencies of constant load. (12) Rectified electrical output of PNG1, PNG2, and PNG3 upon applied biomechanical force press and release polarity test for the PNG3 device. (13) Schematic approach of PNG as a self-powered sensor and its piezoelectric output voltage under different water velocities at an outlet pipe. The inset shows the

DOI: 10.1021/acsami.5b01760
ACS Appl. Mater. Interfaces 2015, 7, 9831−9840

control experimental setup for the active sensor. The Supporting Information is available free of charge on the ACS Publications website at DOI: 10.1021/acsami.5b01760.

AUTHOR INFORMATION

Corresponding Author

*E-mail: kimsangj@jejunu.ac.kr. Fax: 0082-64-756-3886. Phone: 0082−64-754-3715.

Notes

The authors declare no competing financial interest.

ACKNOWLEDGMENTS

This research work was supported by the Basic Science Research Program through the National Research Foundation of Korea (NRF) funded by the Ministry of Science, ICT and Future Planning (2013R1A2A2A01068926).

REFERENCES

(1) Wang, Z. L. Self-Powered Nanosensors and Nanosystems. *Adv. Mater.* **2012**, *24*, 280−285.

(2) Rui, Z.; Lin, L.; Jing, Q.; Wu, W.; Zhang, Y.; Jiao, Z.; Yan, L.; Han, R. P. S.; Wang, Z. L. Nanogenerator as an Active Sensor for Vortex Capture and Ambient Wind-Velocity Detection. *Energy Environ. Sci.* **2012**, *5*, 8528−8533.

(3) Xu, S.; Qin, Y.; Xu, C.; Wei, Y.; Yang, R.; Wang, Z. L. Self-Powered Nanowire Devices. *Nat. Nanotechnol.* **2010**, *5*, 366−373.

(4) Yang, Y.; Zhou, Y.; Wu, J. M.; Wang, Z. L. Single Micro/Nanowire Pyroelectric Nanogenerators as Self-Powered Temperature Sensors. *ACS Nano* **2012**, *6*, 8456−8461.

(5) Yu, A.; Zhao, Y.; Jiang, P.; Wang, Z. L. A Nanogenerator as a Self-Powered Sensor for Measuring the Vibration Spectrum of a Drum Membrane. *Nanotechnology* **2013**, *24*, 055501−055507.

(6) Lin, Z. H.; Cheng, G.; Wu, W.; Pradel, K. C.; Wang, Z. L. Dual-Mode Triboelectric Nanogenerator for Harvesting Water Energy and as a Self-Powered Ethanol Nanosensor. *ACS Nano* **2014**, *8*, 6440−6448.

(7) Liu, H.; Zhang, S.; Kathiresan, R.; Kobayashi, T.; Lee, C. Development of Piezoelectric Micro-Cantilever Flow Sensor with Wind-Driven Energy Harvesting Capability. *Appl. Phys. Lett.* **2012**, *100*, 223905.

(8) Kwon, S. H.; Park, J.; Kim, W. K.; Yang, Y. J.; Lee, E.; Han, C. J.; Park, S. Y.; Lee, J.; Kim, Y. S. An Effective Energy Harvesting Method From a Natural Water Motion Active Transducer. *Energy Environ. Sci.* **2014**, *7*, 3279−3283.

(9) St. Clair, D.; Bibo, A.; Sennakesavababu, V. R.; Daqaq, M. F.; Li, G. A Scalable Concept for Micropower Generation Using Flow-Induced Self-Excited Oscillations. *Appl. Phys. Lett.* **2010**, *96*, 144103.

(10) Wang, Z. L.; Song, J. Piezoelectric Nanogenerators Based on Zinc Oxide Nanowire Arrays. *Science* **2006**, *312*, 242−246.

(11) Hu, Y.; Yang, J.; Jing, Q.; Niu, S.; Wu, W.; Wang, Z. L. Triboelectric Nanogenerator Built on Suspended 3D Spiral Structure as Vibration and Positioning Sensor and Wave Energy Harvester. *ACS Nano* **2013**, *7*, 10424−10432.

(12) Yang, Y.; Guo, W.; Pradel, K. C.; Zhu, G.; Zhou, Y.; Zhang, Y.; Hu, Y.; Lin, L.; Wang, Z. L. Pyroelectric Nanogenerators for Harvesting Thermoelectric Energy. *NanoLett.* **2012**, *12*, 2833−2838.

(13) Yang, J.; You, J.; Chen, C. C.; Hsu, W. C.; Tan, H. R.; Zhang, X. W.; Hong, Z.; Yang, Y. Plasmonic Polymer Tandem Solar Cell. *ACS Nano* **2011**, *5*, 6210−6217.

(14) Shin, S. H.; Kim, Y. H.; Lee, M. H.; Jung, J. Y.; Nah, J. Hemispherically Aggregated $BaTiO_3$ Nanoparticle Composite Thin Film for High-Performance Flexible Piezoelectric Nanogenerator. *ACS Nano* **2014**, *8*, 2766−2773.

(15) Balasubramaniam, S.; Rajneesh, M.; Thiyagarajan, K.; Sang-Jae, K. Fabrication of a ZnO Nanogenerator for Eco-Friendly Biomechanical Energy Harvesting. *RSC Adv.* **2013**, *3*, 16646−16656.

(16) Chang, C.; Tran, V. H.; Wang, J.; Fuh, Y. K.; Lin, L. Direct-Write Piezoelectric Polymeric Nanogenerator with High Energy Conversion Efficiency. *NanoLett.* **2010**, *10*, 726−731.

(17) Wu, J. M.; Chen, K. H.; Zhang, Y.; Wang, Z. L. A Self-Powered Piezotronic Strain Sensor Based on Single $ZnSnO_3$ Microbelts. *RSC Adv.* **2013**, *3*, 25184−25189.

(18) Park, K.-I. P.; Son, J. H.; Hwang, G. T.; Jeong, C. K.; Ryu, J.; Koo, M.; I, Choi.; Lee, S. H.; Byun, M.; Wang, Z. L.; Lee, K. J. Highly-Efficient, Flexible Piezoelectric PZT Thin Film Nanogenerator on Plastic Substrates. *Adv. Mater.* **2014**, *26*, 2514−2520.

(19) Wu, W.; Bai, S.; Yuan, M.; Qin, Y.; Wang, Z. L.; Jing, T. Lead Zirconate Titanate Nanowire Textile Nanogenerator for Wearable Energy-Harvesting and Self-Powered Devices. *ACS Nano* **2012**, *6*, 6231−6235.

(20) Xu, S.; Yeh, Y. W.; Poirier, G. P.; McAlpine, M. C.; Register, R. A.; Nan, Y. Flexible Piezoelectric PMN−PT Nanowire-Based Nanocomposite and Device. *NanoLett.* **2013**, *13*, 2393−2398.

(21) Xia, N.; Fei, W.; Anan, L.; Qi, X.; Zhi, Y.; Yong, Q. Flexible Nanogenerator Based on Single $BaTiO_3$ Nanowire. *Sci. Adv. Mater.* **2013**, *5*, 1−7.

(22) Lin, Z. H.; Yang, Y.; Wu, J. M.; Liu, Y.; Zhang, F.; Wang, Z. L. $BaTiO_3$ Nanotubes-Based Flexible and Transparent Nanogenerators. *J. Phys. Chem. Lett.* **2012**, *3*, 3599−3604.

(23) Yuan, M. M.; Cheng, L.; Xu, Q.; Wu, W. W.; Bai, S.; Gu, L.; Wang, Z.; Lu, J.; Li, H. P.; Qin, Y.; Jing, T.; Wang, Z. L. Biocompatible Nanogenerators through High Piezoelectric Coefficient $0.5Ba(Zr_{0.2}Ti_{0.8})O_3-0.5(Ba_{0.7}Ca_{0.3})TiO_3$ Nanowires for In-Vivo Applications. *Adv. Mater.* **2014**, *26*, 7432−7437.

(24) Wang, Z.; Zhao, K.; Guo, X.; Sun, W.; Jiang, H. L.; Han, X. Q.; Tao, X. T.; Cheng, Z. X.; Zhao, H. Y.; Kimura, H.; Yuan, G. L.; Y, J.; Liu, Z. G. Crystallization, Phase Evolution and Ferroelectric Properties of Sol−Gel-Synthesized $Ba(Ti_{0.8}Zr_{0.2})O_3-x(Ba_{0.7}Ca_{0.3})TiO_3$ Thin Films. *J. Mater. Chem. C* **2013**, *1*, 522−530.

(25) Liu, W. F.; Ren, X. B. Large Piezoelectric Effect in Pb-Free Ceramics. *Phys. Rev. Lett.* **2009**, *103*, 257602−257605.

(26) Fu, H.; Cohen, R. E. Polarization Rotation Mechanism for Ultrahigh Electromechanical Response in Single-Crystal Piezoelectrics. *Nature* **2000**, *403*, 281−283.

(27) Hernandez, B. A.; Chang, K. S.; Fisher, E. R.; Dorhout, P. K. Sol-Gel Template Synthesis and Characterization of $BaTiO_3$ and $PbTiO_3$ Nanotubes. *Chem. Mater.* **2002**, *14*, 480−482.

(28) Scott, J. F. Applications of Modern Ferroelectrics. *Science* **2007**, *315*, 954−959.

(29) Kalyani, A. K.; Senyshyn, A.; Ranjan, R. Polymorphic Phase Boundaries and Enhanced Piezoelectric Response in Extended Composition Range in the Lead Free Ferroelectric $BaTi_{1-x}Zr_xO_3$. *J. Appl. Phys.* **2013**, *114*, 014102/1−6.

(30) Yu, Z.; Ang, C.; Guo, R.; Bhalla, A. S. Piezoelectric and Strain Properties of $Ba(Ti_{1-x}Zr_x)O_3$ Ceramics. *J. Appl. Phys.* **2002**, *92*, 1489−1493.

(31) Li, Z.; Wang, Z. L. Air/Liquid-Pressure and Heartbeat-Driven Flexible Fiber Nanogenerators as a Micro/Nano-Power Source or Diagnostic Sensor. *Adv. Mater.* **2011**, *23*, 84−89.

(32) Hu, Y.; Xu, C.; Zhang, Y.; Lin, Long.; Snyder, R. L.; Wang, Z. L. A Nanogenerator for Energy Harvesting From a Rotating Tire and its Application as a Self-Powered Pressure/Speed Sensor. *Adv. Mater.* **2011**, *23*, 4068−4071.

(33) Yu, A.; Jiang, P.; Wang, Z. L. Nanogenerator as Self-Powered Vibration Sensor. *Nano Energy* **2012**, *1*, 418−423.

(34) Huang, K. C.; Huang, T. C.; Hsieh, W. F. Morphology-Controlled Synthesis of Barium Titanate Nano-Structures. *Inorg. Chem.* **2009**, *48*, 9180−9184.

(35) Li, B. R.; Shang, W.; Hu, Z. L.; Zhang, N. Q. Template-Free Fabrication of Pure Single-Crystalline $BaTiO_3$ Nano-Wires by Molten Salt Synthesis Technique. *Ceram. Int.* **2014**, *40*, 73−80.

(36) Weber, U.; Greuel, G.; Boettger, U.; Weber, S.; Hennings, D.; Waser, R. Dielectric Properties of $Ba(Zr,Ti)O_3$-Based Ferroelectrics for Capacitor Applications. *J. Am. Ceram. Soc.* **2001**, *84*, 759−66.

DOI: 10.1021/acsami.5b01760
ACS Appl. Mater. Interfaces 2015, 7, 9831−9840

(37) Nanakorn, N.; Jalupoom, P.; Vaneesorn, N.; Thanaboonsombut, A. Dielectric and Ferroelectric Properties of $Ba(Zr_xTi_{1-x})O_3$ Ceramics. *Ceram. Int.* **2008**, *34*, 779−782.
(38) Li, W.; Xu, Z.; Chu, R.; Fu, Peng.; Zang, G. Piezoelectric and Dielectric Properties of $(Ba_{1-x}Ca_x)(Ti_{0.95}Zr_{0.05})O_3$ Lead-Free Ceramics. *J. Am. Ceram. Soc.* **2010**, *93*, 2942−2944.
(39) Kim, Y.; Lee, K. Y.; Hwang, S. K.; Park, C.; Kim, S. O.; Cho, J. Layer-by-layer Controlled Perovskite Nanocomposite Thin Films for Piezoelectric Nanogenerators. *Adv. Funct. Mater.* **2014**, *24*, 6262−6269.
(40) Park, K.-I.; Lee, M.; Liu, Y.; Moon, S.; Hwang, G.-T.; Zhu, G.; Kim, J. E.; Kim, S. O.; Kim, D. K.; Wang, Z. L.; Lee, K. J. Flexible Nanocomposite Generator Made of $BaTiO_3$ Nanoparticles and Graphitic Carbons. *Adv. Mater.* **2012**, *24*, 2999−3004.
(41) Han, M.; Zhang, X. S.; Meng, B.; Liu, W.; Tang, W.; Sun, X.; Wang, W.; Zhang, H. r-Shaped Hybrid Nanogenerator with Enhanced Piezoelectricity. *ACS Nano* **2013**, *7*, 8554−8560.
(42) Ricinschi, D.; Ciomaga, C. E.; Mitoseriu, L.; Buscaglia, V.; Okuyama, M. Ferroelectric−Relaxor Crossover Characteristics in $Ba(Zr_xTi_{1-x})O_3$ Ceramics Investigated by AFM-Piezoresponse Study. *J. Eur. Ceram. Soc.* **2010**, *30*, 237−241.
(43) Dong, L.; Donald, S. S.; Lakes, R. S. Enhanced Dielectric and Piezoelectric Properties of $x BaZrO_3$-$(1-x)BaTiO_3$ Ceramics. *J. Appl. Phys.* **2012**, *111*, 084107/1−10.
(44) Wu, J. M.; Xu, C.; Zhang, Y.; Wang, Z. L. Lead-Free Nanogenerator Made from Single $ZnSnO_3$ Microbelt. *ACS Nano* **2012**, *6*, 4335−4340.
(45) Liu, Z. H.; Pan, C. T.; Lin, L. W.; Huang, J. C.; Ou, Z. Y. Direct-Write PVDF Nonwoven Fiber Fabric Energy Harvesters via The Hollow Cylindrical Near-Field Electro Spinning Process. *Smart Mater. Struct.* **2014**, *23*, 025003−025013.
(46) Jeong, C. K.; Park, K.-I.; Ryu, J.; Hwang, G. T.; Lee, K. J. Large-Area and Flexible Lead-Free Nanocomposite Generator Using Alkaline Niobate Particles and Metal Nanorod Filler. *Adv. Funct. Mater.* **2014**, *24*, 2620−2629.
(47) Saravanakumar, B.; Kaliannan, T.; Alluri, N. R.; SoYoon, S.; Taehyun, K.; Lin, Z.-H.; Kim, S.-J. Fabrication of an Eco-Friendly Composite Nanogenerator for Self-Powered PhotoSensor Applications. *Carbon* **2014**, *84*, 56−65.
(48) Zhang, M.; Gao, T.; Wang, J.; Liao, J.; Qiu, Y.; Xue, H.; Shi, Z.; Xiong, Z.; Chenn, L. Single $BaTiO_3$ Nanowires-Polymer Fiber Based Nanogenerator. *Nano Energy* **2015**, 510−517.
(49) Joe, B.; Nimra, J.; Peter, W.; Mark, S.; Paul, M. W.; Markys, C.; Steve, D. Measurement Techniques for Piezoelectric Nanogenerators. *Energy Environ. Sci.* **2013**, *6*, 3035−3045.
(50) Park, K.-I.; Xu, S.; Liu, Y.; Hwang, G. T.; Suk-Joong, L. K.; Wang, Z. L.; Lee, K. J. Piezoelectric $BaTiO_3$ Thin Film Nanogenerator on Plastic Substrates. *Nano Lett.* **2010**, *10*, 4939−4943.
(51) Jeong, C. K.; Kim, I.; Park, K.-I.; Oh, M. H.; Paik, H.; Hwang, G.-T.; No, K.; Nam, Y. S.; Lee, K. J. Virus-Directed Design of a Flexible $BaTiO_3$ Nanogenerator. *ACS Nano* **2013**, *7*, 11016−11025.
(52) Wu, W.; Cheng, L.; Bai, S.; Dou, W.; Xu, Q.; Wei, Z.; Qin, Y. Electrospinning Lead-Free 0.5Ba $(Zr_{0.2}Ti_{0.8})O_3$-$0.5(Ba_{0.7}Ca_{0.3})TiO_3$ Nanowires and Their Application in Energy Harvesting. *J. Mater. Chem. A* **2013**, *1*, 7332−7338.
(53) Pi, Z.; Zhang, J.; Wen, C.; Zhang, Z. B.; Wu, D. Flexible Piezoelectric Nanogenerator Made of Poly(vinylidenefluoride-co-trifluoroethylene) (PVDF-TrFE) Thin Film. *Nano Energy* **2014**, *7*, 33−41.

DOI: 10.1021/acsami.5b01760
ACS Appl. Mater. Interfaces 2015, 7, 9831−9840